Numerical Analysis of the Effect of Grain Size and Defects on the Performance of CIGS Solar Cells

G. Sozzi, F. Troni, R. Menozzi

Department of Information Engineering, University of Parma, V.le G.P. Usberti 181A, 43124 Parma, Italy
roberto.menozzi@unipr.it, Tel. +39-0521-905832

Keywords: solar cells, CIGS, numerical simulation.

Abstract

This work shows two-dimensional numerical simulations aimed at providing indications for the development of optimized thin-film CIGS solar cells. The poly-crystalline nature of CIGS and the presence of defects and Cu-poor regions at the grain boundaries and at the CIGS surface are taken into account, together with the possible displacement of the p-n junction from the CdS/CIGS heterojunction.

INTRODUCTION

Thin-film solar cells based on Cu(In,Ga)Se_2 (CIGS) are experiencing the first phase of commercialization, with a few manufacturers introducing mass production processes yielding cells with efficiencies in the 10-16% range [1]-[3]. Laboratory specimens can provide power conversion efficiency as high as 20% [4], despite the poly-crystalline structure of the semiconductor thin film. The structure of the most popular cells features, from top to bottom, a ZnO transparent contact layer, an n-doped CdS buffer layer, a p-doped CIGS absorber layer, and a backside metal contact sitting on a soda lime glass or flexible substrate.

Several papers were published on material growth, processing and characterization on one side, and on the performance of finished cells and modules on the other, but there is still a gap to fill in between: some of the specific features of CIGS cells, specifically those pertaining to the behavior of grain boundaries and heterojunctions, are still under debate, and a complete understanding of the relationship between material characteristics and cell behavior is not available yet. Since the information about defects, band offsets, potential spikes, etc., at grain boundaries and interfaces is hard to obtain experimentally, and often indirect and speculative, some researchers have tried to bridge the gap using physical-level numerical simulations. This work belongs in this category, as detailed in the following section.

AIM OF THE WORK

By general consensus, the behavior of defects at grain boundaries (GBs), in the grain interior (GI), and at hetero-interfaces is critical for the performance of CIGS solar cells. Therefore, a detailed analysis is important to guide cell design and manufacturing process optimization, since different manufacturing options and process conditions indeed result in widely differing material properties. In particular it is known that: (i) the p-doped CIGS absorber typically has a columnar polycrystalline structure, with grains in the micrometer range; (ii) this polycrystalline structure does not have a disruptive effect on cell performance, probably due to charged defects and/or band offsets preventing the GBs from acting as effective recombination centers [5]; (iii) Cu-poor regions are likely to form at GBs and at the top CIGS interface, resulting in localized wider band-gap and valence band offset – experimental evidence of this phenomenon is given in [6], [7]; (iv) possibly due to Cd migration from the top n-doped CdS layer [8], the metallurgical n-p junction may not coincide with the top CIGS interface, being a buried CIGS-CIGS homo-junction instead.

This contribution builds on simulation works by other groups [9]-[12] and on the available experimental evidence to shed additional light on how the cell performance is impacted by: (1) the CIGS grain size; (2) the presence and thickness of a Cu-poor CIGS interface layer; (3) the depth of the CIGS-CIGS n-p homo-junction. As manufacturers strive for developing new or improved processing technologies for low-cost mass production of CIGS cells and modules, numerical simulations can help forecast what impact different technologies will have on the final cell performance.

NUMERICAL SIMULATIONS

We focus on standard n-ZnO/n-CdS/p-$CuIn_{0.69}Ga_{0.31}Se_2$ cells with columnar polycrystalline CIGS, as illustrated by Fig. 1. Symmetry and periodicity allow to limit the simulated area to one grain boundary, provided that the grain size is reasonably uniform over the cell area. No anti-reflection coating is simulated. All the simulations are performed using the Synopsys Sentaurus suite. The cell behavior in the dark is described by the Poisson, electron and hole continuity, and drift-diffusion equations. Recombination through deep defect levels follows the

Shockley–Read–Hall (SRH) model. Deep traps are located in the GI (bulk acceptors), at the GB (interface donors), and in some simulations at the CIGS/CdS interface (interface donors). The Cu-poor regions (at either the GB or CIGS/CdS interface, or both) feature an increased band-gap totally localized on the valance band, DE_V (i.e., $DE_C = 0$) [6]. Fig. 2 shows the energy band profile along a horizontal line in the vicinity of a GB (with $DE_V = 0.2$ eV). Table I shows the material parameters used in the simulations. The cell is illuminated by the standard AM1.5D solar spectrum.

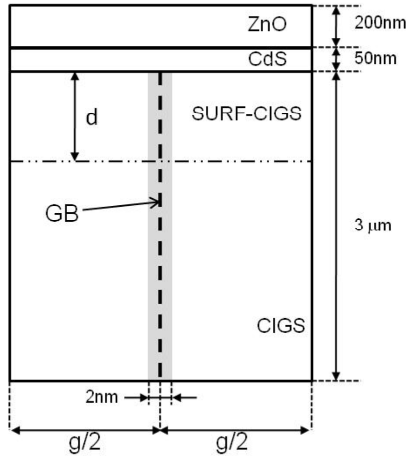

Fig.1 Schematic structure of the simulated solar cell. g is the grain size. The gray shaded region around the GB represents Cu-poor CIGS. A Cu-poor SURF-CIGS layer of thickness d may be present.

TABLE I
MATERIAL PARAMETERS

Layer	ZnO	CdS	CIGS
Eg [eV]	3.3	2.4	1.15
Doping [cm^{-3}]	$N_D = 10^{18}$	$N_D = 6 \cdot 10^{17}$	$N_A = 3 \cdot 10^{17}$
$\varepsilon/\varepsilon 0$	9	10	13.6
m_e/m_0	0.2	0.2	0.09
m_h/m_0	1.2	0.8	0.72
μ_e [$cm^2/(Vs)$]	100	100	100
μ_h [$cm^2/(Vs)$]	25	25	12.5
Bulk traps	**ZnO**	**CdS**	**CIGS**
Density [cm^{-3}]	10^{16}	10^{16}	10^{15}
Energy	midgap	midgap	midgap
σ_e [cm^2]	10^{-16}	10^{-15}	$2 \cdot 10^{-14}$
σ_h [cm^2]	10^{-13}	10^{-12}	$2 \cdot 10^{-14}$
GB traps	**Density**	**Energy [eV]**	**$\sigma_e = \sigma_h$**
Donor	$2 \cdot 10^{12}$ [cm^{-2}]	$E_V + 0.880$	10^{-15} [cm^2]

An example of I-V curve in darkness and under illumination is shown in Fig. 3, where the short-circuit current (J_{SC}) and open-circuit voltage (V_{OC}) are also pointed out.

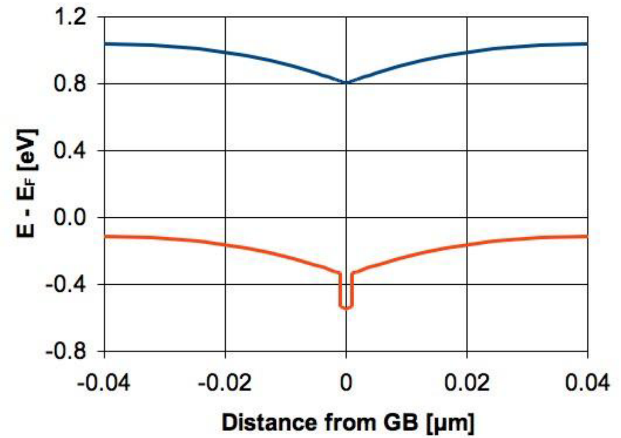

Fig. 2 Energy band profile along a horizontal line in the CIGS (see Fig. 1). The grain boundary is characterized by a valence band offset ΔE_V (0.2 eV in this example).

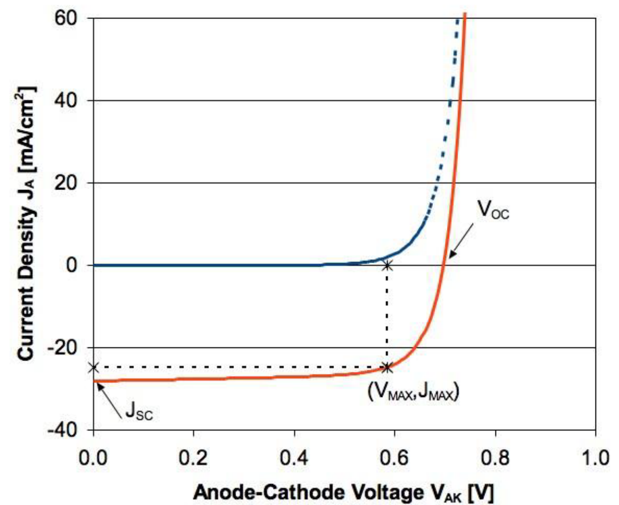

Fig. 3 Dark (dotted line) and illuminated (solid line) diode characteristics. The arrows point to the short-circuit current (J_{SC}) and open-circuit voltage (V_{OC}). (V_{MAX} , J_{MAX}) marks the *maximum power point*. The ratio between $V_{MAX} \cdot J_{MAX}$ and $V_{OC} \cdot J_{SC}$ is called the cell's *fill factor*. The cell's efficiency increases for increasing J_{SC}, V_{OC}, and fill factor.

SIMULATION RESULTS AND DISCUSSION

(1) Effect of the grain size g – Fig. 4 shows the effect of the grain size g on the efficiency η (defined as the ratio between the output power at the maximum power point and the incident radiation power), for three different values of the valence band discontinuity at the GB, ΔE_V. As previously observed, the valence band offset at the GB

hinders hole collection by the GB (see Fig. 2), thus reducing the recombination at GB defects; with DE_V = 0.4 eV the GB is practically passivated; this value is considered excessive by some authors, who claim that a value around 0.2 eV may be closer to physical reality, but there is experimental evidence of band offsets in excess of 0.4 eV [6]. As expected, as the grain size increases, η tends to the single-crystal value higher than 17%. As the grain size is reduced, the diode ideality factor increases (not shown here), indicating that recombination at the GBs plays a significant role. It is interesting to notice that a grain size variation in the 0.5-2 mm range, quite plausible for current manufacturing processes, results in a significant difference in η if the GB is not passivated by a large DE_V.

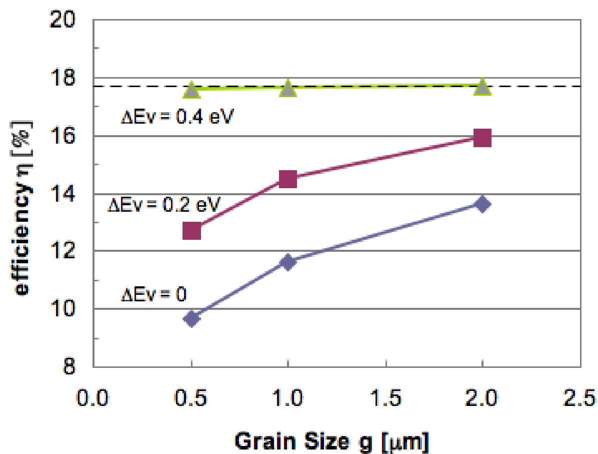

Fig. 4 Effect of CIGS grain size on efficiency, for different values of the valence-band discontinuity at the GB. The dashed line marks the efficiency of the single-crystal cell.

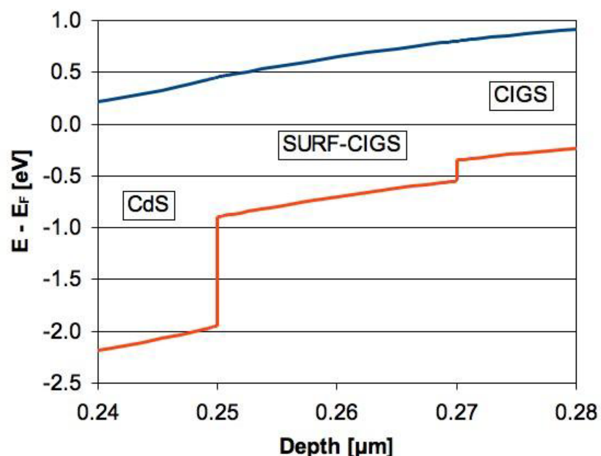

Fig. 5 Equilibrium energy band profile along a vertical line in the presence of a Cu-poor surface CIGS region (SURF-CIGS). The valence band offset at the interface between SURF-CIGS and CIGS is 0.2 eV in this example.

(2) Effect of a surface Cu-poor layer – We simulated the presence of a Cu-poor CIGS layer at the interface with the CdS, by considering a surface CIGS layer (SURF-CIGS) of thickness d (see Fig. 1) with larger band-gap (DE_V = 0.2 eV, DE_C = 0). The energy band profile along a vertical line is shown in Fig. 5. In order to separate the effect of SURF-CIGS from that of GBs, we first considered the case of a single-crystal cell (i.e., without GBs). The effect of d on η is shown in Fig. 6, with and without interface donor traps at the CdS/SURF-CIGS heterojunction. Interestingly, the SURF-CIGS layer improves η, provided that d ≤ 30 nm, due to an increase of the fill factor and V_{OC} (not shown here). This is caused by reduced carrier concentration, hence reduced recombination, in the space-charge region. However, for d ≥ 40 nm, the increase of negative space charge in the depleted p-SURF-CIGS results in hole accumulation at the SURF-CIGS/CIGS interface and larger electron concentration deeper in the CIGS absorber: this increase of minority carrier concentration locally enhances recombination, thus lowering the fill factor (as defined in the caption of Fig. 3) and, consequently, η. In the presence of donor traps at the CdS/SURF-CIGS heterojunction and, therefore, of enhanced space-charge recombination, the presence of SURF-CIGS is even more beneficial.

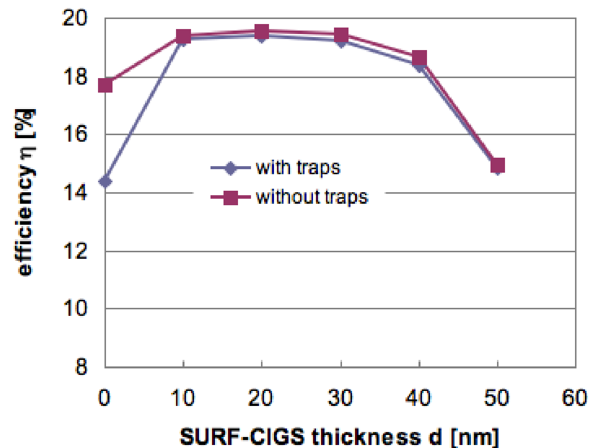

Fig. 6 Effect of the thickness of the Cu-poor surface CIGS layer on the efficiency of a single-crystal cell, with and without donor defects at the CdS/SURF-CIGS interface.

The same considerations apply for cells with GBs. Fig. 7 shows the effect of SURF-CIGS on η as a function of DE_V (the same DE_V is used for the GB and the SURF-CIGS layer) and for different values of d, for a cell with GB size g = 1 mm; the same interface traps are present at the GB and at the CdS/SURF-CIGS interface. η increases with DE_V and d, provided that d < 50 nm.

(3) Effect of the CIGS-CIGS homojunction – There are indications that the position of the p-n junction can be different from that of CdS/CIGS heterojunction [13], possibly due to Cd diffusion from the top n-doped CdS

buffer into p-CIGS. We investigate the effect of the p-n homojunction position, by simulating the structure of Fig. 1 for grain size g = 1 μm, ΔEv = 0.2 eV at the GB/GI interface, and for variable junction depth x_j, both without and with trap states at the CdS/CIGS interface (in the latter case these defects are the same as those at the GB). The efficiency dependence on x_j is shown in Fig. 8 ($x_j = 0$ indicates the ideal situation where the p-n junction and the CdS-CIGS heterojunction coincide). The effect of x_j on η is marginal in the absence of interface traps, but becomes significant if traps are present at the CdS-CIGS interface, because the p-n junction and the space charge region are moved away from an area of increased recombination.

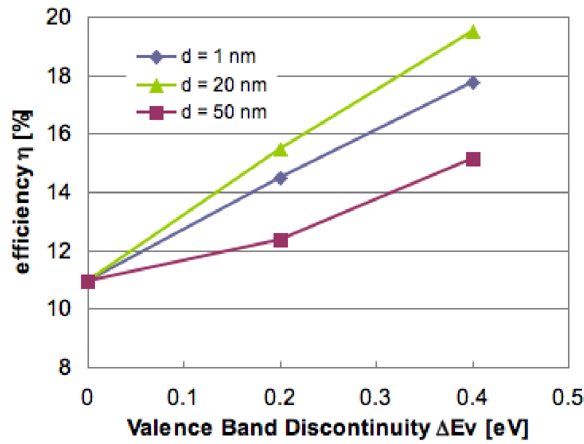

Fig. 7 Effect of the presence of a Cu-poor surface CIGS layer of thickness d. The same valence band discontinuity and the same interface defects are used for the GB and the CdS/SURF-CIGS interface.

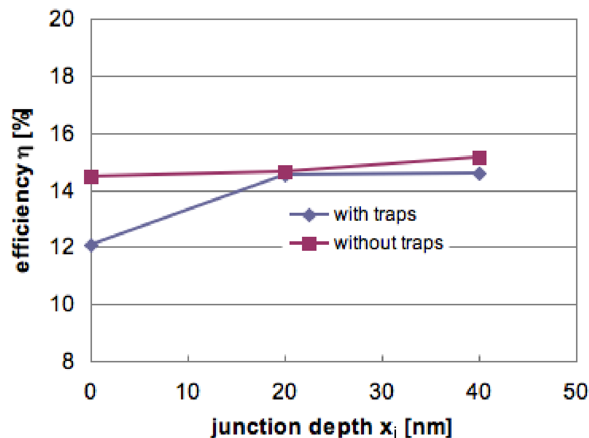

Fig. 8 Effect of the p-n homojunction depth on the cell efficiency, with and without traps at the CdS/CIGS interface. The grain size is 1 μm and $\Delta E_V = 0.2$ eV at the GB.

If we also consider the presence of the SURF-CIGS layer (ΔEv = 0.2 eV), either with or without traps at the CdS-CIGS interface, the effect of the homojunction depth is minor, with η (not shown here) varying by about 1% for x_j ranging between 0 and 40 nm. This is consistent with the observation of point (2) above: the presence of the wider band-gap of SURF-CIGS inhibits surface recombination, thereby reducing the benefit of a deeper p-n junction.

CONCLUSIONS

In conclusion, we have shown results from a campaign of two-dimensional numerical simulations, aimed at providing indications for development and manufacturing of optimized thin-film CIGS solar cells. The poly-crystalline nature of CIGS and the presence of defects and Cu-poor CIGS regions at the grain boundaries and at the interface with the top CdS buffer were taken into account, together with the possible displacement of the p-n junction from the CdS/CIGS heterojunction. These results indicate that detailed physical and electrical characterization of the materials forming the cell stack, particularly in terms of poly-crystalline texture, defects location and nature, is mandatory for quantitative understanding of the cell behavior. Coupled with these experimental data, simulations such as those described here may significantly help understand the impact of different manufacturing processes, affecting grain-size, material composition, and defect nature, location and concentration, on the cell performance.

ACKNOWLEDGEMENTS

Work partly funded by CNR-IMEM, Parma, Italy. The authors would also like to thank the colleagues at CNR-IMEM for fruitful discussions.

REFERENCES

[1] H. Komaki, et al., *33rd IEEE Photovoltaic Specialists Conf.* (2008).
[2] J. S. Britt, et al., *33rd IEEE Photovoltaic Specialists Conf.* (2008).
[3] V. Kapur, et al., *33rd IEEE Photovoltaic Specialists Conf.* (2008).
[4] I. Repins, et al., *Prog. Photovolt.: Res. Appl.*, **16**, pp. 235-239 (2008).
[5] C. Persson and A. Zunger, *Phys. Rev. Lett.*, **91**, 266401 (2003).
[6] M. J. Hetzer, et al., *Appl. Phys. Lett.*, **86**, 162105 (2005).
[7] Z. Zhang, T. Wagner, *Thin Solid Films*, **517**, pp. 4329-4335 (2009).
[8] C.-H. Huang, *J. Phys. Chem. Solids*, **69**, pp. 779-783 (2008).
[9] W. K. Metzger and M. Gloeckler, *J. Appl. Phys.*, **98**, 063701 (2005).
[10] M. Gloeckler, et al., *J. Appl. Phys.*, **98**, 113704 (2005).
[11] K. Taretto and U. Rau, *J. Appl. Phys.*, **103**, 094523 (2008).
[12] U. Rau, et al., *Appl. Phys.* A, **96,** pp. 221-234 (2009).
[13] C.-S. Jiang, et al., *Appl. Phys. Lett.*, **82**, pp. 127-129 (2003).

ACRONYMS

CIGS: Copper Indium Gallium Selenide, $Cu(In,Ga)Se_2$
GB: Grain Boundary
GI: Grain Interior
SRH: Shockley-Read-Hall
AM1.5D: Air Mass 1.5 Direct